Free energy and phase diagram of chromium alloys

R. S. Fishman
Department of Physics, North Dakota State University, Fargo, North Dakota 58105-5566

S. H. Liu
Solid State Division, P.O. Box 2008, Oak Ridge National Lab, Oak Ridge, Tennessee 37831

(Received 3 March 1993)

The phase diagram of chromium alloys is remarkably rich. At the Néel temperature of 310 K, pure chromium undergoes a weakly first-order phase transition into an incommensurate spin-density wave (SDW) state. When doped with more than 0.2% manganese, this transition becomes second order and the SDW becomes commensurate. Over 25 years ago, Koehler *et al.* and Komura, Hamaguchi, and Kunitomi observed a first-order commensurate-to-incommensurate (CI) transition in CrMn alloys. The temperature of this CI transition decreased to zero as the manganese concentration increases from about 0.2% to about 1.5%. Using mean-field theory, we have constructed the free energy and phase diagram of chromium alloys in the presence of electron scattering. In the absence of scattering, the phase diagram allows a first-order phase transition from the incommensurate to the commensurate states with decreasing temperature. But if the damping is sufficiently large, the phase-separation curve flips from the right side of the tricritical point to the left. So within a small window of manganese concentrations, the commensurate state undergoes a first-order transition into the incommensurate state with decreasing temperature, in agreement with the experiments of Koehler *et al.* At zero temperature, we find a first-order phase transition from the incommensurate to the commensurate state with manganese doping, in agreement with the work of Komura, Hamaguchi, and Kunitomi. In the absence of damping, the zero-temperature energy gap $\Delta(0)$ in the commensurate regime is independent of manganese concentration. But in the presence of damping $\Delta(0)$ becomes an increasing function of the manganese concentration.

I. INTRODUCTION

The phase diagram of chromium alloys contains at least four distinct phases.[1-5] At 310 K, pure chromium undergoes a weakly first-order phase transition[2] from a paramagnetic state into a state with an incommensurate spin-density wave (SDW) polarized transverse to its wave vector. At 122 K, the spin flips into the longitudinal direction[1,5] and the magnetic moment of the SDW drops discontinuously. When chromium is doped with more than about 0.2% manganese, the SDW becomes commensurate[4] near the Néel temperature. The temperature of the spin-flip transition decreases with manganese doping[4] and vanishes at about 1% manganese concentration. Early experiments by Koehler *et al.*[4] also revealed that CrMn alloys undergo a first-order commensurate-to-incommensurate (CI) transition. The CI transition temperature decreases to 0 as the manganese concentration increases from about 0.2 to roughly 1.5 %. At zero temperature, Komura, Hamaguchi, and Kunitomi[3] also observed a first-order transition from the incommensurate to the commensurate states with increased manganese doping. Since these measurements were performed over 25 years ago, there has been very little further experimental work on the first-order CI transition. In this paper, we calculate the free energy and phase diagram of chromium alloys, including the effects of electron scattering. Without damping, the phase diagram of chromium alloys admits a first-order transition from the incommensurate-to-commensurate phases. But if the electron damping is sufficiently large, the phase-separation curve flips from one side of the tricritical point to the other and a first-order CI transition occurs within a narrow range of manganese concentrations.

The SDW of chromium is produced by the coherent motion of electrons and holes, which are coupled by the Coulomb attraction $v>0$. In pure chromium, the electron Fermi surface a is slightly smaller than the hole Fermi surface b and both Fermi surfaces are roughly octahedral in shape.[6] As sketched in Fig. 1, the electron and hole Fermi surfaces are imperfectly nested by the wave vector $\mathbf{Q}=G(1-\partial)\hat{\mathbf{z}}/2$, where G is a reciprocal lattice vector and $\partial\approx 0.04$. With manganese or rhenium doping, the size of the electron surface increases, ∂ decreases, and the wave vector Q approaches $G/2$. So the nesting improves. With vanadium doping, on the other hand, the size of the hole surface increases, Q decreases, and the nesting becomes worse.

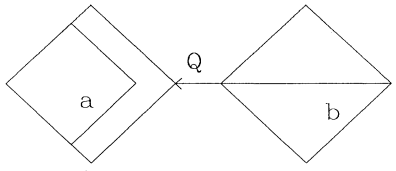

FIG. 1. The imperfect nesting of the electron and hole Fermi surfaces by the wave vector **Q**.

When the hole Fermi surface is translated by $\mp\mathbf{Q}$, the energy mismatch between the resulting hole Fermi surfaces (called $b\pm$) at the Fermi wave vector is given by $z_0 = v_F \partial (2/\sqrt{3}G)$. The energies of the translated Fermi surfaces are shown in Fig. 2. The energy mismatch z_0 is a direct measure of the impurity concentration: z_0 decreases with manganese doping and increases with vanadium doping. For pure chromium, tunneling experiments[7] suggest that z_0 is approximately 450 meV.

Until recently, the wave vector of the SDW was thought to coincide with the nesting wave vector $\mathbf{Q}$. However, we have previously shown[8] that the wave vector of the SDW is actually given by $\mathbf{Q}' = \mathbf{Q} + \mathbf{K}$, where $\mathbf{K} = (G/2)\Lambda\partial\hat{z}$. The dimensionless parameter Λ lies between 0 and 1 and depends on the other model parameters. When $\Lambda = 0$, the SDW wave vector equals the nesting wave vector Q; but when $\Lambda = 1$, $Q' = G/2$ and the SDW is commensurate with the lattice. Translating the hole Fermi surface by $\mathbf{Q}'$ instead of by $\mathbf{Q}$ improves the nesting of the electron and hole surfaces on one side but worsens the nesting on the other side. However, the net condensation energy is always a maximum for some nonzero Λ and wave vector $\mathbf{K}$.

At the Néel temperature, Λ increases with manganese doping and reaches 1 when z_0 equals the tricritical value $z_0^* \approx 2\pi T_N$, which corresponds[4] to about 0.2% manganese concentration. With additional manganese doping, the SDW wave vector remains commensurate with the lattice but the electron Fermi surface continues to catch up in size with the hole Fermi surface and the Néel temperature $T_N(z_0)$ continues to grow.[8] In the absence of damping, the Néel temperature increases until ∂ and z_0 reach zero. This behavior can be found in the phase diagram of Fig. 3. Both the Néel temperature and the energy mismatch z_0 are normalized by T_N^*, which is the Néel temperature in the absence of damping and with $z_0 = 0$. While the commensurate regime lies to the left of the tricritical point, the incommensurate regime lies to the right.

Unlike the nesting wave vector Q, the SDW wave vector may depend on temperature and electron damping. The temperature dependence of Q' was observed by Werner, Arrott, and Kendrick,[5] who found that the SDW wave vector of pure chromium increases monotonically

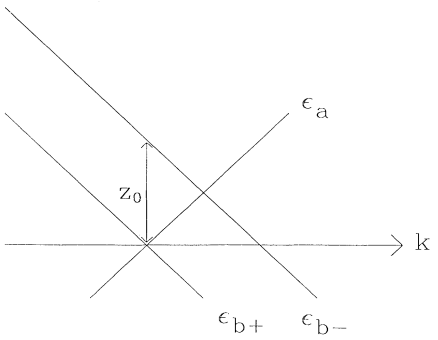

FIG. 2. The energy levels near the Fermi surface for $k_z > 0$, with the hole surface translated by $\mp\mathbf{Q}$.

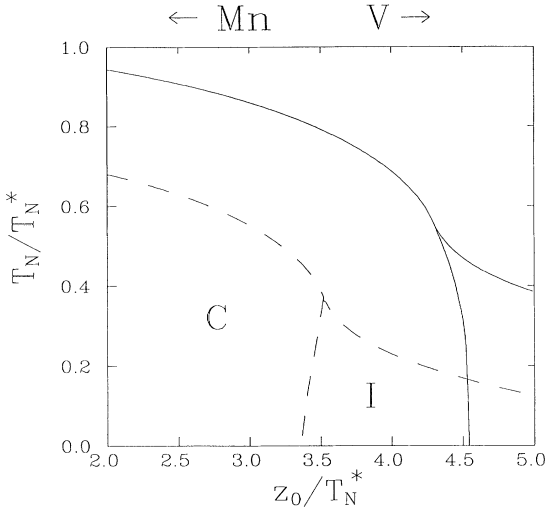

FIG. 3. The phase diagram of chromium alloys with $\Gamma = 0$ (solid) and $\Gamma/T_N^* = 0.3$ (dashed).

with temperature. Within a narrow window of manganese concentrations, the SDW wave vector jumps to $G/2$ at the CI transition.

It is well known that electron scattering plays a very important role in chromium alloys.[4] Because impurities scatter electron and holes with opposite signs, impurity scattering competes with the Coulomb attraction v and suppresses both the SDW order parameter g and the Néel temperature. Due to impurity scattering, the weakly first-order transition in pure chromium becomes second order[9] when the impurity concentration exceeds about 0.2%. In previous work,[8] we have shown that impurity scattering favors the nesting on one side of the Fermi surface at the expense of nesting on the other side. So electron damping tends to decrease the SDW wave vector and to favor the incommensurate over the commensurate states. Of course, damping becomes more effective as thermal fluctuations decrease. In this work, we find that the phase diagram of chromium alloys depends very sensitively on electron damping. Without damping, the phase diagram contains a first-order transition from the incommensurate to the commensurate SDW state; with sufficient damping, the transition goes from the commensurate to the incommensurate state.

In this paper, we construct the free energy and phase diagram of chromium alloys using mean-field theory. While Sec. II treats the case of nonzero temperatures, Sec. III treats the case for $T = 0$. After numerically minimizing these free energies, we construct the phase diagram of chromium alloys in Sec. IV. Finally, Sec. V contains a conclusion. Appendixes A and B contain certain technical details omitted in the text.

II. FINITE-TEMPERATURE FREE ENERGY

The mean-field formalism for chromium alloys was originally developed by Zittartz[10] and Young and Sokoloff[11] for the case $\Lambda = 0$. It is straightforward to general-

ize this formalism to treat the SDW wave vector as a free parameter. The SDW wave vector is then determined by minimizing the mean-field free energy. At the Néel temperature, our results agree with the paramagnetic results of Sato and Maki.[12]

Because the electron and hole surfaces are imperfectly nested, the inverse Green's function of chromium alloys must be written as a 6×6 matrix in spin and band space:

$$\underline{G}^{-1}(\mathbf{k},i\omega_n)=\begin{bmatrix} [i\tilde{\omega}_n^a-\epsilon_a(\mathbf{k})]\underline{1} & -\hat{\mathbf{n}}\cdot\boldsymbol{\sigma}\tilde{g}_n & -\hat{\mathbf{n}}\cdot\boldsymbol{\sigma}\tilde{g}_n \\ -\hat{\mathbf{n}}\cdot\boldsymbol{\sigma}\tilde{g}_n & [i\tilde{\omega}_n^b-\epsilon_{b-}(\mathbf{k})]\underline{1} & 0 \\ -\hat{\mathbf{n}}\cdot\boldsymbol{\sigma}\tilde{g}_n & 0 & [i\tilde{\omega}_n^b-\epsilon_{b+}(\mathbf{k})]\underline{1} \end{bmatrix}, \tag{1}$$

where $\epsilon_a(\mathbf{k})$ is the energy of an electron and $\epsilon_{b\pm}(\mathbf{k})=\epsilon_b(\mathbf{k}\mp\mathbf{Q}')$ are the energies of the holes translated by $\mp\mathbf{Q}'$. Here $\hat{\mathbf{n}}$ is the direction of polarization of the SDW, $\omega_n=\pi T(2n+1)$ are the Matsubara frequencies, $\underline{1}$ is the unit matrix, and $\boldsymbol{\sigma}$ are the Pauli matrices in spin space.

In this work, we neglect the $b+b-$ and $b-b+$ components of $\underline{G}^{-1}(\mathbf{k},i\omega_n)$, which arise from a charge-density wave (CDW) with wave vector $2\mathbf{Q}'$. The CDW is induced[11] by the Coulomb repulsion v' between holes on the $b\pm$ Fermi surfaces. In pure chromium, the first-order phase transition is induced by the proximity to a CDW instability[9] when v' is sufficiently large. We believe that the $b\pm b\mp$ components of the Green's function are primarily important very close to the Néel temperature and will not qualitatively affect the phase diagram of chromium alloys.

The modified SDW order parameter $\tilde{g}_n$ and Matsubara frequencies $\tilde{\omega}_n^{a,b}$ include corrections due to electron scattering. These three complex quantities are evaluated self-consistently in terms of the Green's function from the expressions[10]

$$\hat{\mathbf{n}}\cdot\boldsymbol{\sigma}\tilde{g}_n=\hat{\mathbf{n}}\cdot\boldsymbol{\sigma}g+\frac{\Gamma}{2\pi mk_F}\int_0^\infty p^2dp\,\underline{G}_{ab-}(p,i\omega_n)\,, \tag{2}$$

$$\underline{1}i\tilde{\omega}_n^{a,b}=\underline{1}i\omega_n-\frac{\Gamma}{2\pi mk_F}\int_0^\infty p^2dp\,\underline{G}_{aa,b\pm b\pm}(p,i\omega_n)\,, \tag{3}$$

where

$$\Gamma=\frac{\rho_{sc}k_Fm}{4\pi^2}\int d\Omega|u(\theta)|^2 \tag{4}$$

is the energy width produced by impurity scattering, and $\tau=\hbar/\Gamma$ is the scattering lifetime of electrons and holes near the Fermi surface. In addition, m is the mass of a quasiparticle, k_F is the Fermi wave vector, ρ_{sc} is the density of impurities, and $u(\theta)$ is the impurity potential.

Finally, the self-consistent equation for the SDW order parameter g is given by

$$\begin{aligned}\hat{\mathbf{n}}\cdot\boldsymbol{\sigma}g&=-\frac{v}{2N}T\sum_{n,\mathbf{k}}\{\underline{G}^{b-a}+\underline{G}^{b+a}\}\\&=-\hat{\mathbf{n}}\cdot\boldsymbol{\sigma}\frac{v}{2N}T\sum_{n,\mathbf{k}}\frac{2i\tilde{\omega}_n^b-\epsilon_{b-}-\epsilon_{b+}}{D}\tilde{g}_n\,,\end{aligned} \tag{5}$$

where

$$\begin{aligned}D=&(i\tilde{\omega}_n^a-\epsilon_a)(i\tilde{\omega}_n^b-\epsilon_{b+})(i\tilde{\omega}_n^b-\epsilon_{b-})\\&-\tilde{g}_n^2(2i\tilde{\omega}_n^b-\epsilon_{b-}-\epsilon_{b+})\end{aligned} \tag{6}$$

is the determinant of $\underline{G}(\mathbf{k},i\omega_n)$ and $v>0$ is the attractive Coulomb interaction between the electrons and holes. Of course, the magnetic moment of the SDW is proportional to g.

Near the Fermi surface, the electron and hole energies may be linearized as[6,13]

$$\epsilon_a=z\,, \tag{7a}$$

$$\epsilon_{b+}=\Lambda z_0/2-z\;;\quad k_z>0\,, \tag{7b}$$

$$\epsilon_{b-}=z_0-\Lambda z_0/2-z\;;\quad k_z>0\,. \tag{7c}$$

For $k_z<0$, the expressions for ϵ_{b+} and ϵ_{b-} are reversed. When $\Lambda=0$, the energy mismatch z_0 is given by $\epsilon_{b-}-\epsilon_{b+}$. Now the momentum summations in Eqs. (2), (3), and (5) can be converted into integrals over the energy z and evaluated by factoring the determinant D as

$$D(z)=-(z-z_a)(z-z_{b+})(z-z_{b-})\,. \tag{8}$$

While the imaginary part of z_a has the same sign as ω_n, the imaginary parts of $z_{b\pm}$ have the opposite sign.

After performing the energy integrals, the three complex nonlinear equations for the modified order parameter and frequencies can be rewritten as

$$\tilde{g}_n=g-\frac{i\Gamma}{2}\tilde{g}_n\frac{2i\tilde{\omega}_n^b+2z_a-z_0}{(z_a-z_{b+})(z_a-z_{b-})}\mathrm{sgn}(\omega_n)\,, \tag{9}$$

$$\tilde{\omega}_n^a=\omega_n+\Gamma\left\{\frac{(i\tilde{\omega}_n^b+z_a-\Lambda z_0/2)(i\tilde{\omega}_n^b+z_a+\Lambda z_0/2-z_0)}{(z_a-z_{b+})(z_a-z_{b-})}-\frac{1}{2}\right\}\mathrm{sgn}(\omega_n)\,, \tag{10}$$

$$\tilde{\omega}_n^b=\omega_n+\frac{\Gamma}{2}\left\{\frac{(i\tilde{\omega}_n^a-z_a)(2i\tilde{\omega}_n^b+2z_a+\Lambda z_0/2-z_0)-2\tilde{g}_n^2}{(z_a-z_{b+})(z_a-z_{b-})}+1\right\}\mathrm{sgn}(\omega_n)\,. \tag{11}$$

At the Néel temperature, $\tilde{g}_n=0$ and the modified Matsubara frequencies are identical:

$$\tilde{\omega}_n^a=\tilde{\omega}_n^b=\tilde{\omega}_n\equiv\omega_n+\tfrac{1}{2}\Gamma\,\mathrm{sgn}(\omega_n)\ . \tag{12}$$

Below the Néel temperature, however, $\tilde{\omega}_n^a$ and $\tilde{\omega}_n^b$ differ by terms of order g^2 and higher.

Using the linearized energies, we can also rewrite the self-consistent equation for the order parameter as

$$\frac{g}{T_N^*}\ln\left[\frac{T}{T_N^*}\right]+\sum_{n=0}^{\infty}\left\{\frac{g}{T_N^*}\frac{1}{n+1/2}+2\pi\frac{T}{T_N^*}\mathrm{Re}\left[\tilde{g}_n\frac{2\tilde{\omega}_n^b-2iz_a+iz_0}{(z_a-z_{b+})(z_a-z_{b-})}\right]\right\}=0\ , \tag{13}$$

where T_N^* is the fictitious Néel temperature[12] in the absence of electron scattering and with $z_0=0$. Appendix A provides detailed derivations of Eqs. (9)–(11) and (13).

Finally, we construct the free energy by integrating this self-consistent equation with respect to the order parameter g:

$$\frac{F(g,\Lambda)}{\lambda T_N^*}=\left[\frac{g}{T_N^*}\right]^2\ln\left[\frac{T}{T_N^*}\right]+\sum_{n=0}^{\infty}\left\{\left[\frac{g}{T_N^*}\right]^2\frac{1}{n+1/2}+4\pi\frac{T}{T_N^{*2}}\mathrm{Re}\int_0^g dx\,\tilde{g}_n(x)\frac{2\tilde{\omega}_n^b(x)-2iz_a(x)+iz_0}{[z_a(x)-z_{b+}(x)][z_a(x)-z_{b-}(x)]}\right\}\ , \tag{14}$$

which neglects the constant free energy $F(0,\Lambda)$ of the normal state. All quantities in the integrand above are evaluated with x replacing g. The dimensionless coupling constant λ is given by $\lambda=\rho(\epsilon_F)v/2$, where $\rho(\epsilon_F)$ is the density-of-states at the Fermi surface for a single spin. Of course, minimizing Eq. (14) with respect to g produces the self-consistent expression of Eq. (13).

Because the roots z_i, frequencies $\tilde{\omega}_n^a$ and $\tilde{\omega}_n^b$, and order parameter $\tilde{g}_n$ all depend on the wave vector parameter Λ, it is not possible to construct a simple self-consistent equation for Λ. So in general, $F(g,\Lambda)$ must be minimized with respect to both g and Λ. However, by using the self-consistent equation for g, this minimization can be performed with a single unknown parameter.

At the Néel temperature, the free energy and self-consistent equation can be simplified considerably. To first order in g, $\tilde{g}_n$ is given by

$$\tilde{g}_n=g\frac{(2i\tilde{\omega}_n-\Lambda z_0/2)(2i\tilde{\omega}_n-z_0+\Lambda z_0/2)}{(2i\tilde{\omega}_n-\Lambda z_0/2)(2i\tilde{\omega}_n-z_0+\Lambda z_0/2)+i\Gamma(4i\tilde{\omega}_n-z_0)\mathrm{sgn}(\omega_n)/2}\ , \tag{15}$$

where the frequency $\tilde{\omega}_n$ is given by Eq. (12). It is then straightforward to show that the free energy near the Néel temperature becomes

$$\frac{F(g,\Lambda)}{\lambda T_N^*}=\left[\frac{g}{T_N^*}\right]^2\left\{\ln\left[\frac{T_N}{T_N^*}\right]+\sum_{n=0}^{\infty}\left[\frac{1}{n+1/2}-\mathrm{Re}\left[\frac{X_n}{X_n^2+X_n\rho/2+u^2}\right]\right]\right\}\ , \tag{16}$$

where

$$X_n=n+\tfrac{1}{2}+\tfrac{1}{2}\rho+i\xi\ , \tag{17}$$

$$\rho=\frac{1}{2\pi}\frac{\Gamma}{T}\ , \tag{18}$$

$$\xi=\frac{1}{8\pi}\frac{z_0}{T}\ , \tag{19}$$

$$u=\frac{1}{8\pi}\frac{z_0}{T}(\Lambda-1) \tag{20}$$

are evaluated at T_N. Minimizing this free energy with respect to g and Λ produces the two self-consistent relations

$$\ln\left[\frac{T_N}{T_N^*}\right]+\sum_{n=0}^{\infty}\left\{\frac{1}{n+1/2}-\mathrm{Re}\left[\frac{X_n}{X_n^2+X_n\rho/2+u^2}\right]\right\}=0\ , \tag{21}$$

$$\sum_{n=0}^{\infty}\mathrm{Re}\left\{\frac{X_n}{(X_n^2+X_n\rho/2+u^2)^2}\right\}=0\ ,\quad \Lambda\neq 1\ . \tag{22}$$

When $\Lambda=1$ or the SDW is commensurate, the second expression is not valid. These two relations are identical to those derived by Sato and Maki[12] from the spin susceptibility of the paramagnetic state.

The free energy can also be simplified in the absence of damping, when the modified quantities $\tilde{g}_n$, $\tilde{\omega}_n^a$, and $\tilde{\omega}_n^b$ reduce to their "bare" values. In this limit, the free energy is given by

$$F(g,\Lambda)=\frac{1}{2}\frac{g^2}{T_N^*}-\frac{\nu}{4N}\frac{T}{T_N^*}\sum_{n,\mathbf{k}}\ln\left\{1-g^2\frac{2i\omega_n-\epsilon_{b+}-\epsilon_{b-}}{(i\omega_n-\epsilon_a)(i\omega_n-\epsilon_{b+})(i\omega_n-\epsilon_{b-})}\right\}, \tag{23}$$

which again neglects the constant $F(0,\Lambda)$. Minimizing this free energy with respect to g and Λ yields the expressions

$$\ln\left[\frac{T}{T_N^*}\right]-\sum_{n=0}^{\infty}\left\{\mathrm{Re}\left[\frac{X_n}{X_n^2+u^2}\right]-\frac{1}{n+1/2}\right\}$$
$$=\pi iT\sum_n\left\{\frac{2i\omega_n-z_0+2z_a}{(z_a-z_{b+})(z_a-z_{b-})}-\frac{4i\omega_n-z_0}{(2i\omega_n-z_0/2)^2-z_0^2(\Lambda-1)^2/4}\right\}\mathrm{sgn}(\omega_n), \tag{24}$$

$$2\pi T\sum_n\left\{\frac{2i\omega_n+2z_a-z_0}{(i\omega_n+z_a-z_0/2)^2-z_0^2(\Lambda-1)^2/4}\frac{1}{(z_a-z_{b+})(z_a-z_{b-})}\right\}\mathrm{sgn}(\omega_n)=0, \tag{25}$$

where X_n is now evaluated with $\rho=0$ and for general T. These two expressions are much easier to evaluate than to minimize the general free energy in the presence of damping. Of course, Eqs. (24) and (25) reduce to Eqs. (21) and (22) for g and Λ near the Néel temperature.

III. ZERO-TEMPERATURE FREE ENERGY

In this section, we derive the free energy of chromium alloys at zero temperature. The results of this section provide a useful check on the finite-temperature formalism developed above.

At zero temperature, the sum over Matsubara frequencies is replaced by an integral in the usual way:

$$T\sum_{n=-\infty}^{\infty}f(\omega_n)\to\frac{1}{2\pi}\int_{-\infty}^{\infty}dv\,f(v),$$

for any smooth function $f(v)$. So at $T=0$, the self-consistent relation of Eq. (5) becomes

$$g=\frac{\lambda}{2\pi}\int_{-\infty}^{\infty}dz\int_{-\infty}^{\infty}dv\frac{2i\tilde{v}^b+2z-z_0}{(z-z_a)(z-z_{b+})(z-z_{b-})}\tilde{g}(v), \tag{26}$$

where $\tilde{g}(v)$, $\tilde{v}^a$, and $\tilde{v}^b$ replace $\tilde{g}_n$, $\tilde{\omega}_n^a$, and $\tilde{\omega}_n^b$, respectively, in Eqs. (9)–(11).

Actually, the integral on the right-hand side of Eq. (26) diverges logarithmically as $z\to\pm\infty$. In order to regulate this integral, we subtract from both sides the value of the right-hand side when $g=0$ and $\Gamma=0$. As shown in Appendix B, the divergent integral on the left-hand side of the resulting expression can then be evaluated in terms of T_N^*. The self-consistent equation for the order parameter at $T=0$ is then given by

$$g\left\{\ln[\Lambda(2-\Lambda)]+2\ln\left[\frac{z_0}{T_N^*}\frac{\gamma}{\pi}\right]\right\}=-2\int_0^{\infty}dv\,\mathrm{Re}\left\{\frac{2\tilde{v}^b-2iz_a+iz_0}{(z_a-z_{b+})(z_a-z_{b-})}\tilde{g}+\left[\frac{1}{2v+i\Lambda z_0/2}+\frac{1}{2v+iz_0-i\Lambda z_0/2}\right]g\right\}, \tag{27}$$

where $\ln\gamma\approx0.577$ is Euler's constant.

To construct the $T=0$ free energy, we integrate this self-consistent relation with respect to g:

$$\frac{F(g,\Lambda)}{\lambda T_N^*}=\frac{1}{2}\left[\frac{g}{T_N^*}\right]^2\left\{\ln\left[\frac{z_0^2}{T_N^{*2}}\Lambda(2-\Lambda)\right]+2\ln\left[\frac{\gamma}{\pi}\right]\right\}$$
$$+2\int_0^{\infty}dv\,\mathrm{Re}\left\{\int_0^g dx\frac{2\tilde{v}^b-2iz_a+iz_0}{(z_a-z_{b+})(z_a-z_{b-})}\frac{\tilde{g}}{T_N^{*2}}-\frac{1}{2}\frac{g^2}{T_N^{*3}}\left[\frac{1}{2v+i\Lambda z_0/2}+\frac{1}{2v+iz_0-i\Lambda z_0/2}\right]\right\}. \tag{28}$$

Once again, the integrand of the x integral is evaluated with x in place of g.

In the absence of damping, the $T=0$ order parameter can be evaluated explicitly in the commensurate regime where $\Lambda=1$. As shown in Appendix B,

$$\frac{g(0)}{T_N^*}=\frac{\sqrt{2}}{2}\frac{\pi}{\gamma}\approx1.247\ ;\quad \Lambda=1 \tag{29}$$

is independent of z_0. In this limit, the energy gap $\Delta(0)$ between the electron and hole branches is given by $\sqrt{2}g(0)$. So Eq. (29) yields the BCS-like relation $\Delta(0)=1.764T_N^*$. Since the Néel temperature only reaches T_N^* in the limit $z_0=0$, Eq. (29) also predicts that the ratio $g(0)/T_N$ *decreases* as z_0 decreases or as the nesting improves.

In the presence of damping, $g(0)/T_N^*$ is no longer a

constant in the commensurate regime. As discussed in Sec. IV, $g(0)/T_N^*$ is suppressed by electron damping and increases with decreasing z_0.

IV. PHASE DIAGRAM OF CHROMIUM ALLOYS

The free energies derived in the previous two sections must be minimized with respect to both the wave vector parameter Λ and the order parameter g. As mentioned before, this minimization can be performed numerically with one free parameter by using the self-consistent relations for g. Even so, the numerical calculation is quite demanding.

If electron scattering is absent, the phase diagram of chromium alloys is given by the solid lines in Fig. 3. As shown, the tricritical point is fixed by $z_0/T_N^*=4.291$ and $T_N/T_N^*=0.554$, in agreement with Sato and Maki.[12] At zero temperature, the phase-separation curve between the commensurate and incommensurate states extends to about $z_0/T_N^*=4.53$. Without damping, a first-order incommensurate-to-commensurate (IC) transition occurs with decreasing temperature.

In Fig. 4, we plot the normalized order parameter g/T_N^* versus the normalized temperature T/T_N^* for $\Gamma=0$ and for several different values of z_0/T_N^*. As discussed in Sec. III, the zero-temperature limit of g/T_N^* in the commensurate regime is independent of z_0/T_N^*. But at any nonzero temperature, g/T_N^* decreases with increasing z_0/T_N^*.

The wave vector parameter Λ is plotted versus T/T_N in Fig. 5 for three values of z_0/T_N^* between 4.29 and 4.53. When $z_0/T_N^*=4.5$, the SDW wave vector initially decreases with decreasing temperature. We shall return to this behavior shortly. Remember that as Λ varies between 0 and 1, the SDW wave vector Q' varies between $Q\approx 0.48G$ and $0.50G$. So the change in the SDW with temperature is actually rather small.

Angelescu, Nenciu, and Tonchev[14] and Machida and Fujita[15] obtained similar phase diagrams in the absence of damping. In their work, Machida and Fujita included higher harmonics of the SDW solution. Perhaps as a result, their calculation only produced a second-order transition between the commensurate and incommensurate states. As in this work, Angelescu, Nenciu, and Tonchev only included the first harmonic of the SDW and obtained a first-order IC transition with decreasing temperature in the absence of damping.

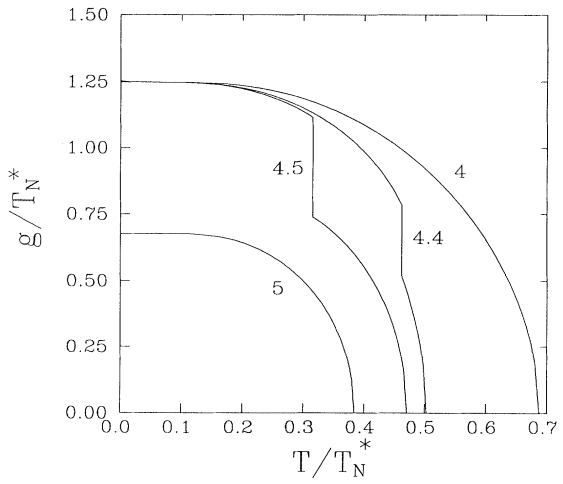

FIG. 4. The normalized order parameter g/T_N^* vs T/T_N^* for $\Gamma/T_N^*=0$ and the four different values of z_0/T_N^* indicated.

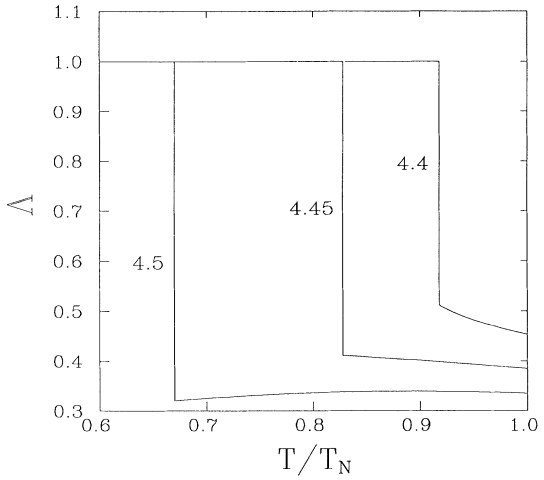

FIG. 5. The wave vector parameter Λ vs T/T_N for $\Gamma/T_N^*=0$ and three different values of z_0/T_N^*.

As anticipated earlier, the phase diagram of chromium alloys depends very sensitively on electron scattering. Because electron damping favors the nesting on one side of the Fermi surface at the expense of the other, it also favors the incommensurate over the commensurate states. In Fig. 1, we find that electron damping may flip the phase-separation curve from one side of the tricritical point to the other. So if the damping energy Γ is sufficiently large, the phase diagram will allow a first-order phase transition from the commensurate to the incommensurate regimes with decreasing temperature.

When $\Gamma/T_N^*=0.3$, the CI transition occurs when z_0/T_N^* lies between 3.36 and the tricritical value of 3.52 or, equivalently, when the manganese impurities lie within a correspondingly narrow window of concentrations. For pure chromium, z_0/T_N^* must be slightly larger than the tricritical value. As shown in Fig. 6, the first-order transition in CrMn alloys is characterized by a discontinuous drop in the order parameter with decreasing temperature. The size of this drop increases with the manganese concentration.

In Fig. 7, we plot the wave vector parameter Λ versus T/T_N for the same two cases. We find that the wave vector Q' jumps discontinuously to $G/2$ with increasing temperature, in agreement with the experimental results of Koehler *et al.*[4] Again, the size of this jump decreases as z_0 increases.

At zero temperature, the order parameter and wave vector change discontinuously with manganese doping as z_0 crosses the phase-separation curve. With $\Gamma/T_N^*=0.3$, the zero-temperature phase transition occurs when z_0 is

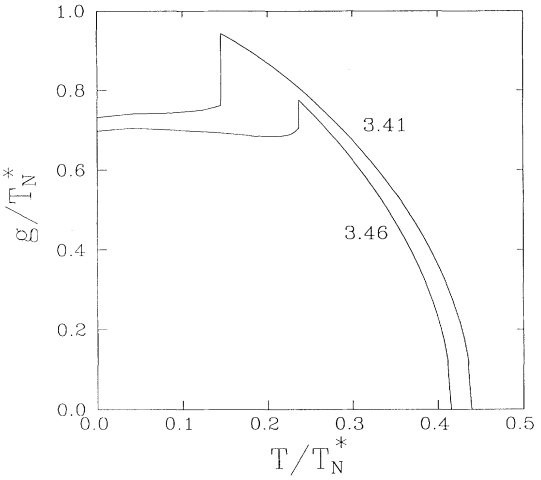

FIG. 6. The normalized order parameter g/T_N^* vs T/T_N^* for $\Gamma/T_N^*=0.3$ and two different values of z_0/T_N^*.

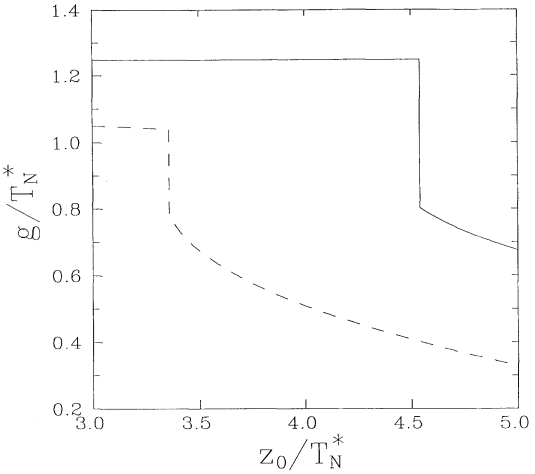

FIG. 8. The $T=0$ normalized order parameter $g(0)/T_N^*$ vs z_0/T_N^* for $\Gamma/T_N^*=0$ (solid) and 0.3 (dashed).

below the tricritical value z_0^*. Experimentally,[4] the tricritical point lies at about 0.2% manganese concentration, while the zero-temperature transition occurs between 1 and 1.5 % manganese concentration.

The normalized order parameter at zero temperature is plotted versus z_0/T_N^* in Fig. 8. In agreement with experiments,[3] the order parameter jumps discontinuously as the manganese concentration increases through the phase-separation curve. Notice that the size of the jump in g/T_N^* decreases with damping. As expected, damping suppresses the zero-temperature order parameter and magnetic moment. In the commensurate regime, $g(0)/T_N^*$ now increases with decreasing z_0. This effect can also be verified from the zero-temperature intercepts of Fig. 6. As for finite temperatures, the first-order change in the order parameter is characterized[4] by hysteresis.

At zero temperature, the wave vector parameter Λ is plotted versus z_0/T_N^* in Fig. 9. For a fixed value of z_0/T_N^*, damping suppresses both Λ and the SDW wave vector. We also find that electron scattering suppresses the jump in the SDW wave vector at the CI transition.

Generally, the magnitude of the SDW free energy is an increasing function of the order parameter g and a decreasing function of the wave vector parameter Λ. As the temperature decreases through the phase-separation curve, the free energy remains constant, while g and Λ both drop discontinuously. As the SDW wave vector continues to decrease in the incommensurate regime, the order parameter may be a nonmonotonic function of temperature, as found in Fig. 6. The slight maxima in g/T_N^* is most pronounced for $z_0/T_N^*=3.46$. Similarly, it is possible for the SDW wave vector to increase with decreasing temperature, so long as the order parameter and the

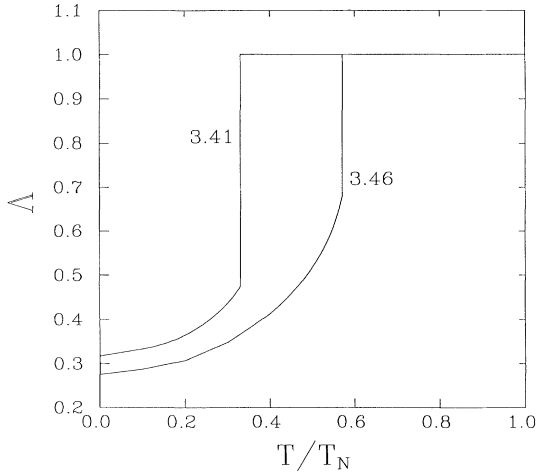

FIG. 7. The wave vector parameter Λ vs T/T_N for the same values of Γ/T_N^* and z_0/T_N^* as in Fig. 6.

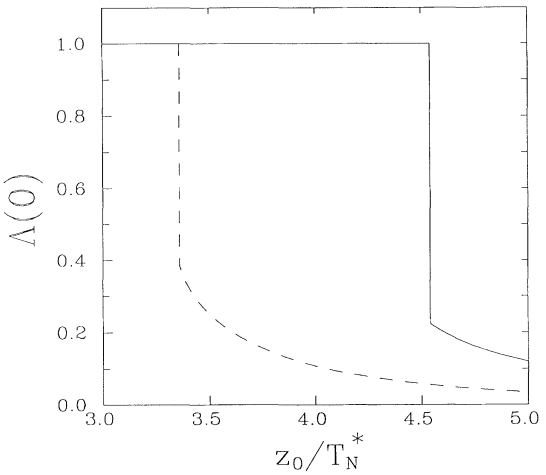

FIG. 9. The $T=0$ wave vector parameter $\Lambda(0)$ vs z_0/T_N^* for the same damping as in Fig. 8.

magnitude of the free energy also grow. This kind of behavior was found in Fig. 5 for $\Gamma=0$ and $z_0/T_N^*=4.5$. By contrast, Angelescu, Nenciu, and Tonchev[14] found that in the absence of damping, the SDW wave vector Q' always decreases with decreasing temperature.

In this work, we have evaluated the phase diagram of chromium alloys for a fixed value of the damping energy. Actually, Γ increases linearly with the density ρ_{sc} of impurities. So it is possible that the incommensurate portion of the phase-separation curve will be larger than indicated in Fig. 3. Because of the importance of electron scattering, a realistic calculation of the phase diagram for chromium alloys must also account for electron-phonon scattering. Since the electron-phonon damping energy Γ_{ph} is proportional to the temperature, we do not expect this form of damping to qualitatively change the shape of the phase diagram.

While this work reveals that electron damping may be responsible for the shape of the phase diagram and the CI transition in CrMn alloys, other factors may also play a role. Angelescu, Nenciu, and Tonchev[14] and Machida and Fujita[15] have found that a finite electron reservoir, which is depleted by the formation of the SDW, can also flip the phase-separation curve from one side of the tricritical point to the other. However, perhaps because their SDW solution contains higher harmonics, Machida and Fujita only obtained a second-order transition from the commensurate-to-incommensurate states. On the other hand, Angelescu, Nenciu, and Tonchev obtained a first-order transition for any value of the reservoir power. By changing the positions of the phase boundaries, the electron reservoir plays a similar role in their calculations that electron damping plays in our work. Of course, both electron damping and a finite electron reservoir may be responsible for the detailed shape of the phase diagram for chromium alloys.

V. CONCLUSIONS

In this paper, we have constructed the mean-field free energy for chromium alloys. If the electron damping is sufficiently large, the phase diagram of chromium alloys contains a first-order transition from the commensurate-to-incommensurate phases with decreasing temperature. Such a phase transition was observed by two groups[3,4] in experiments performed over 25 years ago but has not been duplicated since, as far as we know.

Because of the importance of electron damping, it would be interesting to test the predictions of this paper with isoelectronic impurities such as molybdenum or tungsten. Such impurities increase the damping energy but do not affect the energy mismatch z_0. Because electron scattering favors the incommensurate regime, isoelectronic impurities should enlarge the incommensurate portion of the phase diagram. If T_{CI} is the temperature for the CI transition, then the ratio T_{CI}/T_N should increase with the concentration of molybdenum or tungsten.

Clearly, the condensation free energy alone cannot explain the spin-flip transition in CrMn alloys. This transition occurs below the CI transition and within an even narrower range of manganese concentrations between 0 and about 1%. In at least one sample of 0.35% Mn, Koehler *et al.*[4] observed both the CI and the spin-flip transitions. While the spin-flip transition is also characterized by a discontinuous drop in the order parameter with decreasing temperature, the SDW wave vector does not seem to change through this transition.[5] We believe that the spin-flip transition involves the elastic coupling between the SDW and the lattice. The net condensation and elastic free energies must remain constant across the spin-flip transition.

To conclude, the first-order CI transition in chromium alloys may be produced by electron damping. Hopefully future measurements will test the predictions of this paper and map out the CI phase boundary in this fascinating system.

ACKNOWLEDGMENTS

We would like to acknowledge support from the U.S. Department of Energy under Contract No. DE-AC05-840R21400 with Martin Marietta Energy Systems, Inc. Also, we are grateful for helpful conversations with Douglas Kurtze, Kazumi Maki, and Gen Shirane.

APPENDIX A

In this Appendix, we derive the free energy of chromium alloys for finite temperatures. Our starting points are the complex expressions for $\tilde{g}_n$, $\tilde{\omega}_n^a$, and $\tilde{\omega}_n^b$ given by Eqs. (2) and (3), and the self-consistent relation for g given by Eq. (5). Formally undefined integrals over the energy z must be regulated by multiplying by

$$\lim_{\kappa\to\infty}\frac{\kappa^2}{\kappa^2+z^2}\ .$$

For example,

$$\int_{-\infty}^{\infty}dz\frac{1}{i\omega_n-z}\to\lim_{\kappa\to\infty}\int_{-\infty}^{\infty}dz\frac{1}{i\omega_n-z}\frac{\kappa^2}{(z+i\kappa)(z-i\kappa)}$$
$$=-i\pi\,\mathrm{sgn}(\omega_n)\ . \quad \text{(A1)}$$

The integrals over z are then evaluated using the factorization of the denominator D in Eq. (8). It can be verified that the imaginary parts of two roots always have the opposite sign as ω_n and that the imaginary part of the other root is always the same as ω_n. By construction, the latter root is denoted z_a and the former are labeled $z_{b\pm}$. It is then straightforward to derive Eqs. (9)–(11).

After subtracting off the $g=0$ pieces from both sides of Eq. (5), we obtain the new self-consistent relation

$$gI_1=-\frac{\nu}{2N}T\sum_{n,\mathbf{k}}\left\{\frac{2i\tilde{\omega}_n^b-\epsilon_{b+}-\epsilon_{b-}}{D(g)}\tilde{g}_n-\frac{2i\tilde{\omega}_n-\epsilon_{b+}-\epsilon_{b-}}{D(0)}\left[\frac{\tilde{g}_n}{g}\right]_0 g\right\}, \quad \text{(A2)}$$

$$I_1=1+\frac{\nu}{2N}T\sum_{n,\mathbf{k}}\frac{2i\tilde{\omega}_n-\epsilon_{b+}-\epsilon_{b-}}{D(0)}\left[\frac{\tilde{g}_n}{g}\right]_0, \quad \text{(A3)}$$

where $D(g)$ is the full determinant of Eq. (6), $D(0)$ is the $g=0$ determinant, and $(\tilde{g}_n/g)_0$ is the ratio given by Eq. (15) to zero order in g.

The integral I_1 is logarithmically divergent and must be rewritten as

$$I_1=1-2\lambda T\sum_n\int_{-\epsilon_0}^{\epsilon_0}dz\frac{1}{(z-i\omega_n)(z+i\omega_n)}$$
$$-\lambda T\sum_n\int_{-\infty}^{\infty}dz\left\{\frac{2i\tilde{\omega}_n+2z-z_0}{(z-i\tilde{\omega}_n)(z+i\tilde{\omega}_n-\Lambda z_0/2)(z+i\tilde{\omega}_n+\Lambda z_0/2-z_0)}\left[\frac{\tilde{g}_n}{g}\right]-\frac{2}{(z-i\omega_n)(z+i\omega_n)}\right\}, \tag{A4}$$

where ϵ_0 is an energy cutoff. This cutoff has the same significance as in the BCS theory of superconductivity: Quasiparticles are only well-defined within $\pm\epsilon_0$ of the Fermi energy. This cutoff energy can be exchanged for the Néel temperature T_N^*, which is defined in terms of ϵ_0 and λ by

$$T_N^*=\frac{2\gamma}{\pi}\epsilon_0 e^{-1/2\lambda}. \tag{A5}$$

This expression is also formally identical to the BCS relation for the superconducting transition temperature. As we shall see, neither λ nor ϵ_0 appears explicitly in any final results.

Evaluating the remaining convergent z integrals in I_1 and using Eq. (15) for $(\tilde{g}_n/g)_0$ produces the final result

$$I_1=2\lambda\ln\left[\frac{T}{T_N^*}\right]+2\lambda\sum_{n=0}^{\infty}\left\{\frac{1}{n+1/2}-\mathrm{Re}\left[\frac{X_n}{X_n^2+X_n\rho/2+u^2}\right]\right\}, \tag{A6}$$

which employs the definitions in Eqs. (17)–(20). Finally, performing the z integral on the right-hand side of Eq. (A2) produces the self-consistent relation of Eq. (13), which does not contain either ϵ_0 or λ.

APPENDIX B

In this Appendix, we derive the self-consistent equation for g and the free energy at $T=0$. Our starting point is the self-consistent expression given by Eq. (26). After subtracting from both sides the value of the right-hand side when $g=0$ and $\Gamma=0$, we obtain

$$gI_2=\frac{\lambda}{2\pi}\int_{-\infty}^{\infty}dz\int_{-\infty}^{\infty}dv\left\{\frac{2i\tilde{v}^b+2z-z_0}{(z-z_a)(z-z_{b+})(z-z_{b-})}\tilde{g}+\frac{2iv+2z-z_0}{(iv-z)(iv+z-\Lambda z_0/2)(iv+z+\Lambda z_0/2-z_0)}g\right\}, \tag{B1}$$

$$I_2=1+\frac{\lambda}{2\pi}\int_{-\epsilon_0}^{\epsilon_0}dv\int_{-\infty}^{\infty}dz\frac{2iv+2z-z_0}{(iv-z)(iv+z-\Lambda z_0/2)(iv+z+\Lambda z_0/2-z_0)}, \tag{B2}$$

where the cutoff energy has the same significance as in Appendix A.

After performing the z integral in I_2, we obtain

$$I_2=1-i\lambda\int_0^{\epsilon_0}dv\left\{\frac{1}{2iv-\Lambda z_0/2}+\frac{1}{2iv+\Lambda z_0/2-z_0}\right\}$$
$$+i\lambda\int_{-\epsilon_0}^{0}dv\left\{\frac{1}{2iv-\Lambda z_0/2}+\frac{1}{2iv+\Lambda z_0/2-z_0}\right\}. \tag{B3}$$

Then after performing the v integral, we impose the condition that the energy cutoff ϵ_0 is much larger than the energy mismatch z_0:

$$I_1=1-\lambda\ln\left[\frac{4\epsilon_0}{\Lambda z_0}\right]-\lambda\ln\left[\frac{4\epsilon_0}{(\Lambda-2)z_0}\right]$$
$$=2\lambda\ln\left[\frac{\gamma}{\pi}\right]+\lambda\ln\left[\frac{z_0^2\Lambda(\Lambda-2)}{4T_N^{*2}}\right], \tag{B4}$$

which uses the definition of T_N^* in Eq. (A5). Finally, after evaluating the z integral on the right-hand side of Eq. (B1), we obtain the self-consistent expression of Eq. (27).

When $\Gamma=0$, the zero-temperature self-consistent equation for the order parameter given by Eq. (26) can be rewritten as

$$1=-\frac{\lambda}{\pi}\int_{-\epsilon_0}^{\epsilon_0}dz\int_{-\infty}^{\infty}dv\frac{1}{(iv-z)(iv+z-z_0/2)-2g^2}. \tag{B5}$$

After evaluating the v integral, we find

$$1=\lambda\int_{-\epsilon_0}^{\epsilon_0}dz\frac{1}{\sqrt{(z-z_0/4)^2+2g^2}}. \tag{B6}$$

So for $\epsilon_0\gg z_0$ and $z_0<4\sqrt{2}g$,

$$1=2\lambda\ln\left[\frac{2\epsilon_0}{\sqrt{2}g}\right] \tag{B7}$$

or $g(0)=(\pi/\gamma\sqrt{2})T_N^*$, as given by Eq. (29).

[1]G. Shirane and J. Takei, J. Phys. Soc. Jpn. **17**, 35 (1962).
[2]A. Arrott, S. A. Werner, and H. Kendrick, Phys. Rev. Lett. **14**, 1022 (1965).
[3]S. Komura, Y. Hamaguchi, and N. Kunitomi, J. Phys. Soc. Jpn. **23**, 171 (1967).
[4]W. C. Koehler, R. Moon, A. L. Trego, and A. R. MacKintosh, Phys. Rev. **151**, 405 (1966).
[5]S. Werner, A. Arrott, and H. Kendrick, Phys. Rev. **155**, 528 (1967).
[6]L. M. Falicov and D. R. Penn, Phys. Rev. **158**, 476 (1967).
[7]M. A. Lind and J. L. Stanford, Phys. Lett. **39A**, 5 (1972).
[8]R. S. Fishman and S. H. Liu, Phys. Rev. B **47**, 11 870 (1993).
[9]R. S. Fishman and S. H. Liu, Phys. Rev. B **45**, 12 306 (1992).
[10]J. Zittartz, Phys. Rev. **164**, 575 (1967).
[11]C. Y. Young and J. B. Sokoloff, J. Phys. F **4**, 1304 (1974).
[12]H. Sato and K. Maki, Int. J. Magn. **4**, 163 (1973); **6**, 183 (1974).
[13]The energy ζ used in Ref. 8 is given by $\zeta = z_0 \Lambda / 2$.
[14]N. Angelescu, G. Nenciu, and N. S. Tonchev, J. Phys. F **14**, 2155 (1984).
[15]K. Machida and M. Fujita, Phys. Rev. B **30**, 5284 (1992).